Intestinal AMPK modulation of microbiota mediates cross-talk with brown fat to control thermogenesis

Wendong Huang (whuang@coh.org)
Diabetes and Metabolism Research Institute, Beckman Research Institute, City of Hope National Medical Center

Eryun Zhang
Institute of Diabetes and Metabolism Research Institute, Beckman Research Institute, City of Hope National Medical Center

Lihua JIN
Institute of Diabetes and Metabolism Research Institute, Beckman Research Institute, City of Hope National Medical Center

Yangmeng Wang
Institute of Diabetes and Metabolism Research Institute, Beckman Research Institute, City of Hope National Medical Center

Jui Tu
Institute of Diabetes and Metabolism Research Institute, Beckman Research Institute, City of Hope National Medical Center

Lili Ding
Shanghai University of Traditional Chinese Medicine

Zhipeng Fang
Institute of Diabetes and Metabolism Research Institute, Beckman Research Institute, City of Hope National Medical Center https://orcid.org/0000-0001-5720-1709

Mingjie Fan
Institute of Diabetes and Metabolism Research Institute, Beckman Research Institute, City of Hope National Medical Center

Ismail Al-Abdullah
Department of Translational Research & Cellular Therapeutics, Beckman Research Institute, City of Hope National Medical Center

Rama Natarajan
Beckman Research Institute of City of Hope, Diabetes Metabolism Research Institute
https://orcid.org/0000-0003-4494-1788

Ke Ma
Institute of Diabetes and Metabolism Research Institute, Beckman Research Institute, City of Hope National Medical Center

Zhengtao Wang

Shanghai University of Traditional Chinese Medicine

Arthur Riggs

City of Hope

Li Yang

Shanghai University of Traditional Chinese Medicine

Research Article

Keywords: Brown Adipose tissue, Nutrient Processing, Thermogenic Regulation, Anti-microbial Peptide Controlled Gut Microbiota

Posted Date: January 26th, 2021

DOI: https://doi.org/10.21203/rs.3.rs-117974/v1

Version of Record: A version of this preprint was published at Nature Communications on March 3rd, 2022. See the published version at https://doi.org/10.1038/s41467-022-28743-5.

Intestinal AMPK modulation of microbiota mediates cross-talk with brown fat to control thermogenesis

Eryun Zhang[1,2], Lihua Jin[2], Yangmeng Wang[2], Jui Tu[2,3], Lili Ding[1, 2], Zhipeng Fang[2], Mingjie Fan[2], Ismail Al-Abdullah[4], Rama Natarajan[2], Ke Ma[2], Zhengtao Wang[1], Art Riggs[2], Li Yang[1*], Wendong Huang[2,3*]

[1]Shanghai Key Laboratory of Compound Chinese Medicines and The Ministry of Education (MOE) Key Laboratory of Standardization of Chinese Medicines, Institute of Chinese Materia Medica, Shanghai University of Traditional Chinese Medicine, Shanghai, China.

[2]Department of Diabetes Complications & Metabolism, Diabetes and Metabolism Research Institute, Beckman Research Institute, City of Hope National Medical Center, Duarte, CA.

[3]Graduate School of Biological Science, City of Hope National Medical Center, Duarte, CA.

[4]Department of Translational Research & Cellular Therapeutics, Diabetes and Metabolism Research Institute, Beckman Research Institute, City of Hope National Medical Center, Duarte, CA.

* Correspondence should be addressed to L.Y. (yl7@shutcm.edu.cn) and W.H. (whuang@coh.org).

The energy-dissipating capacity of brown adipose tissue through thermogenesis can be targeted to improve energy balance[1,2]. Mammalian 5′-AMP-activated protein kinase (AMPK), a key nutrient sensor for maintaining cellular energy status[3-5], is a known therapeutic target for glucose control in Type II diabetes (T2D)[6,7]. Despite current understandings of its well-established roles in regulating glucose metabolism in various tissues[4,8-10], the functions of AMPK in the intestine, an organ for nutrient processing, remain largely unexplored. Using an intestinal epithelium-specific AMPK-null (AMPK-IKO) mouse model, we demonstrated that AMPK in the intestine communicated with brown adipose tissue (BAT) to promote thermogenesis. Mechanistically, we uncovered a novel link between intestinal AMPK activation and BAT thermogenic regulation through modulating anti-microbial peptide (AMP)-controlled gut microbiota and the metabolites. Our findings identified a new AMPK-mediated mechanism of intestine-BAT communication that may partially underlie the therapeutic effects of AMPK activator metformin (N, N-dimethylbiguanide).

Improvements of glucose control by AMPK activators, including metformin, AICAR (5-aminoimidazole-4-carboxamide riboside), resveratrol, and Cucurbitacin B, are accompanied by the activation of AMPK signaling in the intestine[11-17], suggesting a significant contribution of intestinal AMPK in global glucose homeostasis. However, the specific function of AMPK in the intestine in overall energy balance and glucose metabolism remain largely unexplored. To address this current knowledge gap in our understanding of AMPK action, we genetically ablated AMPKα1, the predominant AMPK α subunit, selectively in the intestinal epithelial cells (IECs) (**Supplementary Fig. 1a**)[18,19]. On normal chow diet (NC), the IEC-specific AMPK knockout (AMPK-IKO) mice did not exhibit an overt developmental or metabolic phenotypes as compared to $AMPK^{fl/fl}$ mice (**Supplementary Fig. 1b-h**). Surprisingly, however, BAT sections from AMPK-IKO mice displayed marked adipocyte hypertrophy with more abundant multilocular lipid droplets than that of the controls (**Fig. 1a**). Further analysis revealed consistent down-regulation of the thermogenic gene program, including key regulators UCP1 (uncoupling protein 1), ADRB3 (adrenoceptor beta 3), PGC-1α (peroxisome proliferator-activated receptor gamma coactivator

1-alpha), and Dio2 (iodothyronine deiodinase 2). Consistent with the impaired thermogenic program, genes involved in mitochondrial function, fatty acid oxidation, and lipolysic pathways, were significantly attenuated in the BAT of AMPK-IKO mice (**Fig. 1b**). UCP1 protein level was markedly reduced in the BAT of AMPK-IKO mice than that of control $AMPK^{fl/fl}$ mice, both at room temperature and under cold exposure (**Fig. 1c**). Further corroborating these findings, indirect calorimetry assay demonstrated a ~50% reduction of energy expenditure in intestinal AMPK-null mice at ambient temprature, as indicated by oxygen consumption (VO_2) and carbon dioxide production (VCO_2) rate (**Fig. 1d-e, Supplementary Fig. 1i-l**). Consistent with the attenuated thermogenic program leading to lower heat production, AMPK-IKO mice displayed lower rectal temperatures than $AMPK^{fl/fl}$ mice under cold exposure (**Fig. 1f**).

We next tested the response of intestinal AMPK in regulating energy balance when challenged by over-nutrition using a diet-induced obese (DIO) mouse model. Despite similar food intake on the high-fat diet (HFD), AMPK-IKO mice gained significantly more weight than $AMPK^{fl/fl}$ mice (**Fig. 1g, Supplementary Fig. 1m-n**), and developed markedly impaired glucose and insulin tolerance as compared to $AMPK^{fl/fl}$ mice (**Fig. 1h-k**). In line with previous obervations, attenuated energy balance and glucose metabolism were accompanied by suppression of thermogenic program and UCP1 protein expression in BAT (**Fig. 1l-m**), together with markedly lower energy expenditure (**Fig. 1n-o, Supplementary Fig. 1o-r**). These results indicate a protective function of intestinal AMPK againt over-nutrition through maintenance of BAT thermogenic regulation.

Recent reports indicate that changes in gut microbiota can modulate BAT thermogenesis and whole-body energy expenditure[20-22]. Intriguingly, as oral administration of AMPK activators metformin and ber-berine alters gut microbiota composition[23], intestinal AMPK may mediate cross-talk with BAT through regulatory effects on gut microbiota profile. We thus profiled gut microbiota in AMPK-IKO and $AMPK^{fl/fl}$ mice on a NC diet. Significantly altered gut microbiota in AMPK-IKO mice was observed as compared to that of $AMPK^{fl/fl}$ mice (**Fig. 2a, Supplementary Fig. 2**), including the abundance of bacteria species

known to modulate glucose, lipid, and energy metabolism (**Fig. 2b**). Thus, gut microbiota may mediate specific functions of intestinal AMPK in metabolism.

To further confirm that gut microbiota mediates intestinal AMPK action in metabolic homeostasis, we performed fecal microbiota transplantation (FMT) using microbiota harvested from AMPK-IKO mice. FMT from AMPK-IKO, as compared to FMT from $AMPK^{fl/fl}$ mice, led to markedly increased lipid accumulation in BAT sections as indicated by more abundant lipid droplets (**Fig. 2c**). Consistently, the thermogenic gene program genes and related pathways of BAT function, together with UCP1 protein, were all significantly reduced in the BAT of mice received FMT from AMPK-IKO (**Fig. 2d-e**). Further corroborating these observations, when the recipient mice were exposed to 6°C for 2 h, mice that received FMT from AMPK-IKO had significantly lower rectal temperatures (**Fig. 2f**), suggesting impaired heat production. This result was further supported by the functional gene profile of BAT of mice under cold exposure (**Supplementary Fig. 3**). Together, these results indicate that gut microbiota from AMPK-IKO mice is sufficient to impair BAT thermogenesis, suggesting that intestinal AMPK may confer its regulation of BAT through gut microbiota.

Gut microbiota primarily regulate BAT thermogenic funcions through their metabolites[24-27]. we thus conducted a metabolomic analysis of serum samples from DIO AMPK-IKO and $AMPK^{fl/fl}$. Indeed, intestinal AMPK deficiency led to significantly altered serum metabolites (**Fig. 2g**). Methylglyoxal, one of the altered metabolites produced by intestinal bacteria and host metabolism, was of particular interest due to its high levels in diabetic patients and known involvement in development of T2D[28-32]. We further confirmed the significantly higher methylglyoxal levels in AMPK-IKO mice compared to $AMPK^{fl/fl}$ mice by ELISA (**Fig. 2h**). Notably, FMT from AMPK-IKO mice was able to increase methylglyoxal levels in recipient mice (**Fig. 2i**), suggesting that increased production of methylglyoxal by gut microbiota due to loss of intestinal AMPK can be transferred by FMT. We then directly tested the potential of methylglyoxal on modulating thermogenic regulation in brown adipocytes using the HIB1B cell line. Indeed, methylglyoxal

induced significant suppression of UCP1 protein in a dose-dependent manner in differentiated HIB1B cells (**Fig. 2j**). Various pathways related to BAT function was also reduced by methylglyoxal treatment (**Supplementary Fig. 4**). Furthermore, we show that oral gavage of mice with methylglyoxal reduced UCP1 expression in BAT (**Fig. 2k**) and induced lipid accumulation in brown adipocytes (**Fig. 2l**), suggesting direct effect of methylglyoxal on lowering BAT activity both in brown adipocyte and *in vivo*. In aggregate, these data indicate that gut microbiota metabolites, particularly methylglyoxal, could mediate the crosstalk between intestinal AMPK action and BAT thermogenic regulation.

AMPs, the gut-bacterial-derived peptides, have been shown to effectively kill pathogens[33] to maintain an effective barrier against microbes on intestinal epithelium. Considering the critical role of AMPs in determining microbiota composition and markedly altered microbiota profile of AMPK-IKO mice, we postulate that AMPK action in the intestine may directly modulate AMP expression. Interestingly, we found markedly reduced mRNA and protein levels of Reg3γ, a key AMP, in the intestinal tissue of AMPK-IKO mice than in that of $AMPK^{fl/fl}$ mice (**Fig. 3a-b**). Moreover, expression of several other AMPs, including Reg3β, RELMβ (resistin-like molecule β), MMP7 (matrix metallopeptidase 7), and Defa (α-defensin), were similarly reduced by loss of AMPK (**Fig. 3a, Supplementary Fig. 5a**). In contrast, treatment by AMPK activator AICAR directly induced AMP expression in human epithelial HT-29 cells (**Supplementary Fig. 5b**). Reg3γ in the gut can directly target bacteria by attacking peptidoglycan carbohydrate backbone of both Gram-positive and Gram-negative species[34,35]. We therefore chose to further examine Reg3γ regulation by AMPK as a key representative AMP. AMPK activators AICAR and metformin induced Reg3α transcript (the human homolog of mouse Reg3γ) in HT-29 cells in a dose-dependent manner (**Fig. 3c-d**); whereas AMPK knockdown impaired these effects (**Fig. 3e-g**). Furthermore, metformin strongly restored Reg3γ expression in the small intestines of $AMPK^{fl/fl}$ mice but not AMPK-IKO mice (**Fig. 3h**), providing support that Reg3 expression is directly controlled by AMPK signaling. Most importantly, in obese patients with T2D, we observed significantly reduced Reg3α expression, together with evidence of attenuated intestinal AMPK expression and T172 phosphorylation sug-

123 gestive of its activity (**Fig. 3i**). Taken together, these findings identify an unexpected role of intestinal
124 AMPK in modulating gut microbiota composition through regulation of AMPs, such as Reg3γ, in both
125 rodents and humans.
126
127 Metformin is a first-line anti-diabetes drug [36-38] and accumulating evidence indicate its action in the gut
128 is important to glucose control[12,39-41]. However, the underlying molecular mechanisms of this contribu-
129 tion remain unclear. Strikingly, as shown in **Fig 4a and 4e,** the effect of metformin on inducing body
130 weight loss in DIO-AMPK$^{fl/fl}$ mice (**Fig. 4a**) was largely abolished in the AMPK-IKO (**Fig. 4e**). Notably,
131 similar reduction of metformin effect on improving glucose tolerance (**Fig. 4b and 4f**), hepatic lipid ac-
132 cumulation (**Fig. 4c and 4g**), and reducing fasting serum levels of triglycerides and total cholesterol
133 (**Fig. 4d and 4h**), were also observed, indicating that these metabolic actions of metformin are depend-
134 ent on intestinal AMPK (**Fig. 4a-h, Supplementary Fig. 6a-b**).
135
136 Although AMPK is expressed in BAT and metformin can enhance AMPK activity in BAT to activate
137 brown fat thermogenic activity[42-44], whether intestinal AMPK could contribute to the effects of metformin
138 in BAT is yet to be tested. We found that metformin reduced lipid accumulation and UCP1 level in the
139 BAT of AMPK$^{fl/fl}$, but not AMPK-IKO mice (**Fig. 4i-j**), supporting the idea that AMPK action in the gut is
140 required for metformin regulation of BAT function. Interestingly, prior studies indicate that metformin
141 alters the gut microbiota of obese and diabetic patients[45-47], which may contribute to the therapeutic ef-
142 fects of metformin. In line with these findings, we found that metformin treatment significantly altered
143 the relative amount of several bacterial genera in AMPK$^{fl/fl}$, while this effect is lost in AMPK-IKO mice
144 (**Fig. 4k, Supplementary Fig. 6c-d**), suggesting that the metformin-controlled alteration of gut microbi-
145 ota depends on intestinal AMPK. As expected, metformin induced Reg3γ expression in the intestines of
146 AMPK$^{fl/fl}$ but not AMPK-IKO mice (**Fig. 3h**). Taken together, these results suggest that the metabolic
147 effects of AMPK-activating metformin is dependent on AMPK function in the gut, likely through an intes-
148 tinal AMPK-AMP-gut microbiota link.

The role of AMPK in cellular energy homeostasis is highly essential and conserved in eukaryotes. The intestine plays a central role in nutrient sensing, absorption, and metabolism. Our current study reveals for the first time that the cross-talk between intestinal AMPK and BAT regulates thermogenesis and metabolism through modulating AMP-controlled gut microbiota and the metabolites. Thus, our findings provide a new mechanistic underpinning of AMPK function in metabolic regulation, which may shed light on the ongoing large clinical trials of metformin, as well as general drug discoveries utilizing enteral drug administration to treat metabolic diseases.

ACKNOWLEDGEMENTS

We thank Dr. Fouad Kandeel, Dr. Debbie Thurmond, and Dr. Qiong (Annabel) Wang for their helpful discussions. We particularly thank Dr. Kerin Higa for reviewing and editing the manuscript. This study was supported in part by the Schaeffer Foundation, the Hench Foundation, the National Institutes of Health (grants R01CA139158 and R01DK124627 to W.H. and COH P30CA33572), the National Natural Science Foundation of China (grants 81303186 and 81573581 to L.Y.), and the International Postdoctoral Exchange Fellowship Program of China (to E.Z.).

AUTHOR CONTRIBUTIONS

W.H. conceptualized and designed the experiments, wrote and revised the manuscript. E.Z., L.Y. and L.J. designed the experiments, analyzed data, wrote and revised the manuscript. E.Z. performed most of the experiments. Y.W., J.T., L.D., Z.F., and M.F. helped obtain the *in vivo* data. K.M., I.A., Z.W., R.N. and A.R. provided conceptual input and edited the manuscript.

COMPETING FINANCIAL INTERESTS

The authors declare no competing financial interests.

Online METHODS

Clinical samples. Duodenal mucosa specimens were collected from patients with obesity and T2D at the Southern California Islet Cell Resource Center at City of Hope. In brief, subjects were divided into an obese with diabetes group (n=5) and a non-obese, non-diabetic group (n=5). Obesity was defined as a body mass index of 30 or greater, and T2D was defined according to the stringent HbA1c guidelines established by the American Diabetes Association (T2D: HbA1c >6.5%, approximately equivalent to 7.8 mM blood glucose) (**Supplementary Table 1**). All participants provided written informed consent, and ethical approval for this study was granted by the Institutional Review Board of City of Hope (IRB No. 01046).

Animals. Wild-type (WT) C57BL/6J, C57BL/6-AMPKa1$^{flox/flox}$ mice (#014141), and B6.Cg-Tg (Vil-cre) 1000Gum/J (#021504) were purchased from Jackson Laboratory (Bar Harbor, ME). AMPK-IKO mice were generated by cross-breeding C57BL/6-AMPKa1$^{flox/flox}$ mice with B6.Cg-Tg (Vil-cre) 1000Gum/J. All animal procedures were approved by the City of Hope Institutional Animal Care and Use Committee and conducted in accordance with the National Institutes of Health Guidelines for the Care and Use of Laboratory Animals. 8-12-week-old male mice were used in the animal experiments (unless otherwise indicated). Mice were housed in a temperature (22-23°C) and light-controlled vivarium with free access to water and normal chow diet (NC) (17% kcal fat; Diet 8640, Harlan Teklad, Madison, WI) or high-fat diet (HFD, 60% kcal fat; D12492, Research Diets, New Brunswick, NJ). HFD was started at 6 weeks of age and continued for 12 weeks. All treatment groups were weight-matched and randomized to treatment groups at the initiation of each experiment. Cold exposure was performed at 6°C in a light- and humidity-controlled (40%) climatic chamber under specific-pathogen-free (SPF) conditions. To assess whole-body energy metabolism, mice were placed into metabolic cages and acclimatized for approximately 48 h. Food and fluid intake, ambient locomotor activity, O2 consumption (VO_2), CO2 output (VCO_2), respiratory exchange ratio (RER), and energy expenditure were measured using a Comprehensive Laboratory Animal Monitoring System (Columbus Instruments). Body composition was meas-

ured using magnetic resonance imaging (EchoMRI, Houston, TX). To investigate the effects of methylglyoxal on BAT activity, mice were treated with intraperitoneal (i.p.) injections of methylglyoxal (50 mg/kg) once daily for 14 days. For chronic metformin studies, 6-week-old male AMPK$^{fl/fl}$ and AMPK-IKO mice were switched from ND chow to HFD for 6 weeks. Then, they were weight-matched and divided into two groups to receive vehicle treatment (tap water) or metformin by oral gavage (100 mg/kg) once daily for 8 weeks.

Metabolic phenotype and blood measurements. To test glucose tolerance, mice were fasted for 16 h before i.p. injection of glucose solution (1.5 mg/g body weight). Blood glucose levels were measured at baseline and at 15, 30, 60, and 120 min post-injection using an Accu-Chek glucometer (Roche Diagnostics, France). To test insulin tolerance, mice were fasted for 4 h before i.p. injection of insulin (0.75 U/kg body weight). Blood glucose levels were measured at baseline and at 15, 30, 60, and 120 min post-injection. Serum methylglyoxal levels were determined using a Methylglyoxal ELISA Kit (abcam, Cambridge, MA). Serum insulin was assessed after a 12 h of fasting using a Mouse Insulin ELISA Kit (Millipore Sigma, Burlington, MA) according to the manufacture's instructions. Plasma triglyceride and total cholesterol levels were determined using LabAssay Triglyceride and Cholesterol Kits (Wako Chemicals, Osaka, Japan), respectively.

Gut microbiota profiling. Bacterial DNA was extracted from the cecal contents of mice using a QIAamp DNA Stool Mini Kit (Qiagen). The V4 region of the bacterial 16S rRNA gene was amplified by triplicate PCR (F515/R806) using barcoded fusion primers. Samples were pooled in sets of a maximum of 96 samples in equal quantities. Paired-end sequencing of the amplicon library was performed on the Illumina MiSeq 300-bp paired-end platform. A multi-step bioinformatics analysis performed using QIIME 1.9.1 software included filtering raw fastq files for primer and adaptor dimer sequences, removing contaminating host sequences and chimeric sequences, clustering sequences into operational taxonomic units (OTUs) using the open reference OTU calling method with the greengenes 16S reference, and

calculating alpha and beta diversity metrics. Non-metric multidimensional scaling (NMDS) is an ordination technique that aims to discover data patterns in N-dimensional space. It represents the major variation among objects in a reduced dimensional space. Linear discriminant analysis (LDA) of effect size (LEfSe) and the cladogram method were used for microbial biomarker discovery. The data were analyzed on the free online Majorbio Cloud Platform (www.majorbio.com).

Fecal microbiota transplantation (FMT). FMT was performed as described in a previous study [48]. In brief, 8-week-old WT recipient mice were treated with a cocktail of antibiotics, including metronidazole, vancomycin, neomycin, and ampicillin to deplete their gut flora. First, they were administered the antibiotic cocktail in drinking water (per 1 L of water: 1 g metronidazole, 500 mg vancomycin, 1 g neomycin, and 1 g ampicillin) for one week. Then, they were orally gavaged with 200 μl of the antibiotic cocktail (per 1mL of water: 0.5 g metronidazole, 0.5 g vancomycin, 0.5 g neomycin, and 0.5 g ampicillin) once daily for another week. Fresh feces were collected from donor mice under SPF conditions. Feces samples were weighed and diluted with 1 ml of saline per 0.1 g of stool, steeped for about 15 min, shaken, and then centrifuged at 800 g for 3 min. The supernatant was obtained for gavage.

Histology analysis. Tissues were fixed in 10% formalin and were paraffin-embedded. Multiple sections (5 mm) were prepared and stained with hematoxylin and eosin (H&E) for general morphological observation.

Serum metabolomics. Serum metabolic profiling was conducted using ultra-high-performance liquid chromatography (HPLC) (Waters, Milford, USA) coupled with a TripleTOF 5600+ mass spectrometer (Applied Biosystems, USA). A total of 2,007 metabolite peaks were measured. Of those, 485 were structurally identified and annotated using an in-house LC-MS/MS database. Clusters of coabundant metabolites were identified using the dynamic hybrid tree-cutting algorithm (R package: dynamic-

TreeCut), with a deepSplit value of 4 and a minimum cluster size of 2. Metabolites that did not fit the clustering criteria were regarded as singletons.

Cell culture. HIB1B brown pre-adipocytes were cultured in Dulbecco's modified Eagle's medium (DMEM; Thermo Fisher, Pittsburg, PA, USA) supplemented with 10% fetal bovine serum (Atlas Biologicals, Fort Collins, CO, USA) and 1% penicillin–streptomycin (Thermo Fisher). After reaching confluence, cell differentiation was induced using high-glucose DMEM containing 10% FBS, 20 nM insulin, 1 nM triiodothyronine (T3), 0.5 mM IBMX, and 1 μM dexamethasone for 2 days. Cells were re-fed every other day with DMEM containing 10% fetal bovine serum and insulin and T3 at the same concentrations listed above. From the 1st day of the differentiation process, cells were treated with various concentrations of methylglyoxal. The HT-29 cell line was obtained from ATCC and cultured in McCoy's 5a medium supplemented with 10% fetal bovine serum and 1% penicillin–streptomycin.

IEC isolation. Mice were sacrificed after anesthesia, and the small intestine was immediately removed and flushed from both ends with sterile PBS. The small intestine was then opened longitudinally and washed thoroughly with cold PBS. The tissue was then incubated in 10 ml of PBS containing 30 mM EDTA and 1.5 mM dithiothreitol on ice for 20 min, washed in cold PBS, and incubated in 10 ml of PBS containing 30 mM EDTA at 37°C on a shaker (200 rpm) for 10 min. Then, the samples were shaken vigorously for 30 s and centrifuged at 1000 × *g* for 5 min at 4°C. Cell pellets were washed with PBS containing 10% FBS and collected for experiments.

AMPK knockdown in cells. HT-29 cells were transfected with siRNA targeting *PRKAA1* (sc-45312, Santa Cruz Biotechnology) or a control siRNA (SIC001, Sigma) using Lipofectamine 3000 (11668–027, Invitrogen) according to the manufacturer's instructions. Cells were incubated for 24 h with a transfection mixture containing a final siRNA concentration of 100 pM and then supplemented with fresh medium.

Western blot analysis. 20 μg of cells or 40 μg of tissue lysates were subjected to electrophoresis on 10% acrylamide gels and transferred to PVDF membranes. The membranes were incubated for 1 h with blocking buffer (either TBS-T containing 5% [w/v] BSA or 5% skim milk). The membranes were then incubated with the indicated primary antibodies diluted in blocking buffer (1:1,000) for 12 h at 4°C: anti-pAmpk-α Thr172 (Cell Signaling, #2535s), anti-Ampk-α (Cell Signaling, #2532), anti-UCP1 (abcam, ab10983), anti-Reg3γ (R&D, 3873), and anti-Reg3α (abcam, ab202057). The membranes were washed three times with TBS-T and incubated with the appropriate secondary HRP-conjugated antibodies (diluted 1:2,000 in 5% skim milk) at room temperature for 1 h. Finally, the membranes were washed in TBS-T three times for 10 min each, and the signal was detected using enhanced chemiluminescence reagent (Pierce, IL, USA). Protein levels were quantified by densitometry using Image J software.

RT-PCR analysis. Total RNA was extracted from tissues and cells using TRIzol reagent, according to the manufacturer's instructions. The purity and concentration of the total RNA were determined using a NanoDrop spectrophotometer (ND-1000, Thermo Fisher). 1 μg of total RNA was reverse transcribed using cDNA Synthesis SuperMix (Invitrogen, CA, USA). Quantitative real-time PCR was carried out using an ABI 7900HT Fast Real-Time PCR System (Applied Biosystems, Warrington, UK) with SYBR Green PCR Master Mix (Applied Biosystems) and gene-specific primers (**Supplementary Table 2**). The sequences and GenBank accession numbers of the forward and reverse primers used to quantify mRNA are listed in Supplementary Table S2. Relative mRNA levels were normalized against Gapdh.

Statistical analysis. Statistical analyses were performed using GraphPad Prism (version 8). All data are expressed as mean ± s.e.m. One-way analysis of variance (ANOVA) with Tukey's post-hoc tests was used to determine the statistical significance of differences between multiple groups. Student's t-tests were used to determine the statistical significance of differences between two groups. $P < 0.05$ was considered statistically significant.

REFERENCES

1. Calvani, R., Leeuwenburgh, C. & Marzetti, E. Brown adipose tissue and the cold war against obesity. *Diabetes* **63**, 3998-4000 (2014).
2. Virtanen, K.A.*, et al.* Functional brown adipose tissue in healthy adults. *The New England journal of medicine* **360**, 1518-1525 (2009).
3. Lin, S.C. & Hardie, D.G. AMPK: Sensing Glucose as well as Cellular Energy Status. *Cell Metabolism* **27**, 299-313 (2018).
4. Hardie, D.G. & Sakamoto, K. AMPK: a key sensor of fuel and energy status in skeletal muscle. *Physiology (Bethesda)* **21**, 48-60 (2006).
5. Inoki, K., Kim, J. & Guan, K.L. AMPK and mTOR in cellular energy homeostasis and drug targets. *Annual review of pharmacology and toxicology* **52**, 381-400 (2012).
6. Carling, D. AMPK signalling in health and disease. *Current Opinion in Cell Biology* **45**, 31-37 (2017).
7. Steinberg, G.R. & Carling, D. AMP-activated protein kinase: the current landscape for drug development. *Nature reviews. Drug discovery* **18**, 527-551 (2019).
8. Mottillo, E.P.*, et al.* Lack of Adipocyte AMPK Exacerbates Insulin Resistance and Hepatic Steatosis through Brown and Beige Adipose Tissue Function. *Cell Metab* **24**, 118-129 (2016).
9. Cokorinos, E.C.*, et al.* Activation of Skeletal Muscle AMPK Promotes Glucose Disposal and Glucose Lowering in Non-human Primates and Mice. *Cell metabolism* **25**, 1147-1159 e1110 (2017).
10. Woods, A.*, et al.* Liver-Specific Activation of AMPK Prevents Steatosis on a High-Fructose Diet. *Cell reports* **18**, 3043-3051 (2017).
11. Harmel, E.*, et al.* AMPK in the small intestine in normal and pathophysiological conditions. *Endocrinology* **155**, 873-888 (2014).
12. Duca, F.A.*, et al.* Metformin activates a duodenal Ampk-dependent pathway to lower hepatic glucose production in rats. *Nat Med* **21**, 506-511 (2015).
13. Cote, C.D.*, et al.* Resveratrol activates duodenal Sirt1 to reverse insulin resistance in rats through a neuronal network. *Nature Medicine* **21**, 498-U284 (2015).
14. Walker, J.*, et al.* 5-aminoimidazole-4-carboxamide riboside (AICAR) enhances GLUT2-dependent jejunal glucose transport: a possible role for AMPK. *Biochem J* **385**, 485-491 (2005).
15. Sakar, Y.*, et al.* Metformin-induced regulation of the intestinal D-glucose transporters. *J Physiol Pharmacol* **61**, 301-307 (2010).
16. Bauer, P.V.*, et al.* Metformin Alters Upper Small Intestinal Microbiota that Impact a Glucose-SGLT1-Sensing Glucoregulatory Pathway. *Cell Metabolism* **27**, 101-+ (2018).
17. Kim, K.H.*, et al.* Cucurbitacin B Induces Hypoglycemic Effect in Diabetic Mice by Regulation of AMP-Activated Protein Kinase Alpha and Glucagon-Like Peptide-1 via Bitter Taste Receptor Signaling. *Front Pharmacol* **9**, 1071 (2018).
18. Sun, X., Yang, Q., Rogers, C.J., Du, M. & Zhu, M.J. AMPK improves gut epithelial differentiation and barrier function via regulating Cdx2 expression. *Cell Death Differ* **24**, 819-831 (2017).
19. Duca, F.A., Bauer, P.V., Hamr, S.C. & Lam, T.K. Glucoregulatory Relevance of Small Intestinal Nutrient Sensing in Physiology, Bariatric Surgery, and Pharmacology. *Cell Metab* **22**, 367-380 (2015).
20. Yuan, T.*, et al.* Effects of metformin on metabolism of white and brown adipose tissue in obese C57BL/6J mice. *Diabetol Metab Syndr* **11**, 96 (2019).

21. Chevalier, C.*, et al.* Gut Microbiota Orchestrates Energy Homeostasis during Cold. *Cell* **163**, 1360-1374 (2015).
22. Turnbaugh, P.J.*, et al.* An obesity-associated gut microbiome with increased capacity for energy harvest. *Nature* **444**, 1027-1031 (2006).
23. Zhang, X.*, et al.* Modulation of gut microbiota by berberine and metformin during the treatment of high-fat diet-induced obesity in rats. *Sci Rep* **5**, 14405 (2015).
24. Canfora, E.E., Meex, R.C.R., Venema, K. & Blaak, E.E. Gut microbial metabolites in obesity, NAFLD and T2DM. *Nat Rev Endocrinol* **15**, 261-273 (2019).
25. Li, Z.*, et al.* Butyrate reduces appetite and activates brown adipose tissue via the gut-brain neural circuit. *Gut* **67**, 1269-1279 (2018).
26. Hu, J.*, et al.* Short-Chain Fatty Acid Acetate Stimulates Adipogenesis and Mitochondrial Biogenesis via GPR43 in Brown Adipocytes. *Endocrinology* **157**, 1881-1894 (2016).
27. Mills, E.L.*, et al.* Accumulation of succinate controls activation of adipose tissue thermogenesis. *Nature* **560**, 102-106 (2018).
28. Mancabelli, L.*, et al.* Unveiling the gut microbiota composition and functionality associated with constipation through metagenomic analyses. *Scientific reports* **7**, 9879 (2017).
29. Matafome, P., Rodrigues, T., Sena, C. & Seiça, R. Methylglyoxal in Metabolic Disorders: Facts, Myths, and Promises. *Medicinal Research Reviews* **37**, 368-403 (2017).
30. Booth, I.R.*, et al.* Bacterial production of methylglyoxal: a survival strategy or death by misadventure? *Biochemical Society transactions* **31**, 1406-1408 (2003).
31. Moraru, A.*, et al.* Elevated Levels of the Reactive Metabolite Methylglyoxal Recapitulate Progression of Type 2 Diabetes. *Cell metabolism* **27**, 926-934.e928 (2018).
32. Jia, X. & Wu, L. Accumulation of endogenous methylglyoxal impaired insulin signaling in adipose tissue of fructose-fed rats. *Molecular and cellular biochemistry* **306**, 133-139 (2007).
33. Ageitos, J.M., Sanchez-Perez, A., Calo-Mata, P. & Villa, T.G. Antimicrobial peptides (AMPs): Ancient compounds that represent novel weapons in the fight against bacteria. *Biochem Pharmacol* **133**, 117-138 (2017).
34. Loonen, L.M.*, et al.* REG3gamma-deficient mice have altered mucus distribution and increased mucosal inflammatory responses to the microbiota and enteric pathogens in the ileum. *Mucosal Immunol* **7**, 939-947 (2014).
35. Cash, H.L., Whitham, C.V., Behrendt, C.L. & Hooper, L.V. Symbiotic Bacteria Direct Expression of an Intestinal Bactericidal Lectin. *Science (New York, N.Y.)* **313**, 1126-1130 (2006).
36. Zhou, G.*, et al.* Role of AMP-activated protein kinase in mechanism of metformin action. *The Journal of clinical investigation* **108**, 1167-1174 (2001).
37. Madiraju, A.K.*, et al.* Metformin suppresses gluconeogenesis by inhibiting mitochondrial glycerophosphate dehydrogenase. *Nature* **510**, 542-546 (2014).
38. Luo, T.*, et al.* AMPK Activation by Metformin Suppresses Abnormal Extracellular Matrix Remodeling in Adipose Tissue and Ameliorates Insulin Resistance in Obesity. *Diabetes* **65**, 2295-2310 (2016).
39. McCreight, L.J., Bailey, C.J. & Pearson, E.R. Metformin and the gastrointestinal tract. *Diabetologia* **59**, 426-435 (2016).
40. Rena, G., Hardie, D.G. & Pearson, E.R. The mechanisms of action of metformin. *Diabetologia* **60**, 1577-1585 (2017).
41. Stepensky, D., Friedman, M., Raz, I. & Hoffman, A. Pharmacokinetic-pharmacodynamic analysis of the glucose-lowering effect of metformin in diabetic rats reveals first-pass pharmacodynamic effect. *Drug Metab Dispos* **30**, 861-868 (2002).

42. van Dam, A.D., Kooijman, S., Schilperoort, M., Rensen, P.C. & Boon, M.R. Regulation of brown fat by AMP-activated protein kinase. *Trends Mol Med* **21**, 571-579 (2015).
43. Yang, Q.*, et al.* AMPK/alpha-Ketoglutarate Axis Dynamically Mediates DNA Demethylation in the Prdm16 Promoter and Brown Adipogenesis. *Cell metabolism* **24**, 542-554 (2016).
44. Breining, P.*, et al.* Metformin targets brown adipose tissue in vivo and reduces oxygen consumption in vitro. *Diabetes Obes Metab* **20**, 2264-2273 (2018).
45. Wu, H.*, et al.* Metformin alters the gut microbiome of individuals with treatment-naive type 2 diabetes, contributing to the therapeutic effects of the drug. *Nature medicine* **23**, 850-858 (2017).
46. Bryrup, T.*, et al.* Metformin-induced changes of the gut microbiota in healthy young men: results of a non-blinded, one-armed intervention study. *Diabetologia* **62**, 1024-1035 (2019).
47. Forslund, K.*, et al.* Disentangling type 2 diabetes and metformin treatment signatures in the human gut microbiota. *Nature* **528**, 262-266 (2015).
48. Chang, C.J.*, et al.* Ganoderma lucidum reduces obesity in mice by modulating the composition of the gut microbiota. *Nat Commun* **6**, 7489 (2015).

Figure 1

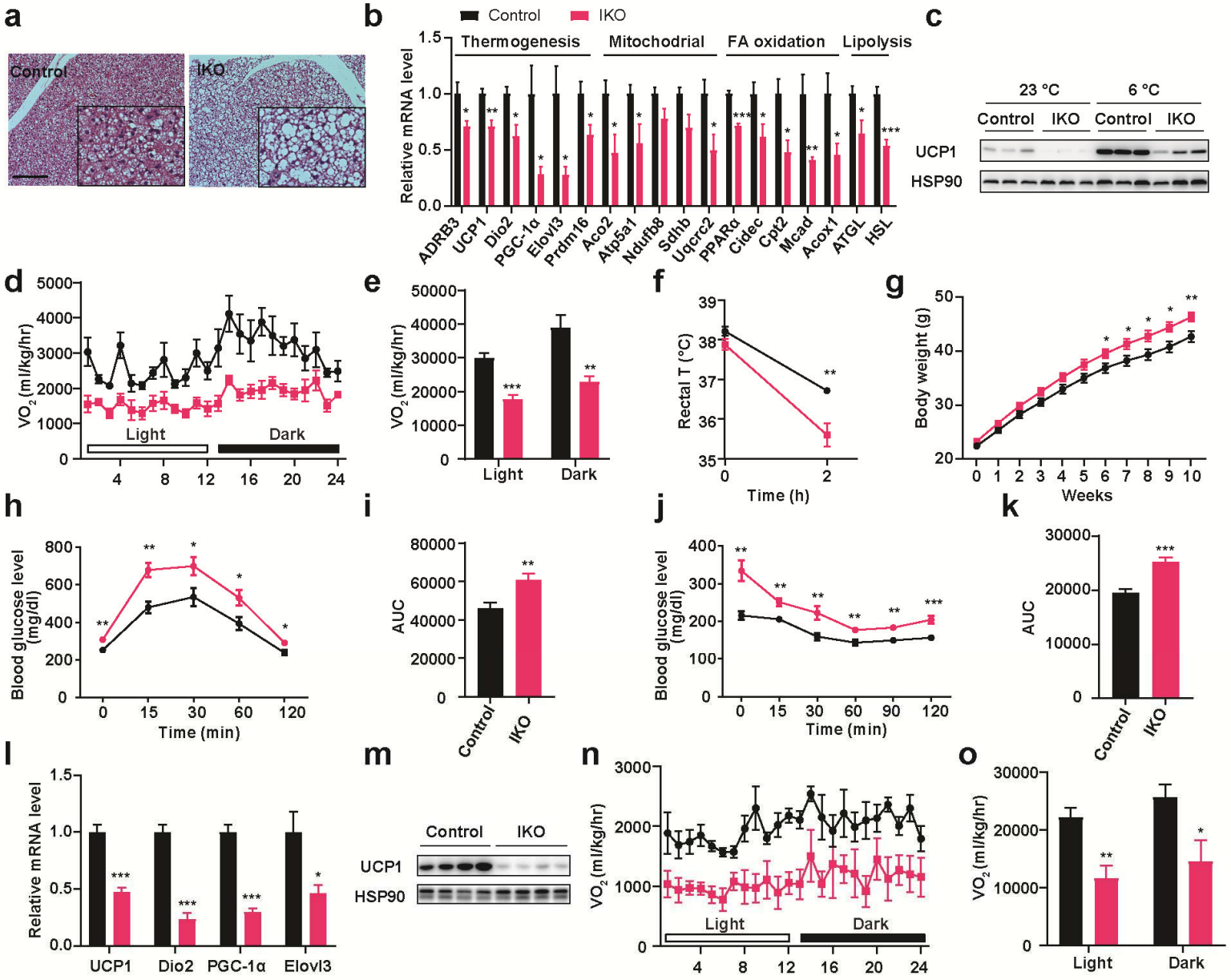

Figure 1. **Intestinal epithelial AMPK knockout mice have impaired BAT function**. For a-f, AMPK$^{fl/fl}$ (Control) and AMPK-IKO mice were fed NC. (a) Representative images of H&E-stained BAT sections. Scale bar =100 μm. (b) Relative mRNA levels of genes in BAT, detected by qPCR (n=5). (c) Western blot analysis of UCP1 protein levels in BAT before and after cold exposure (6° C) for 1 week. (d-e) VO_2 of mice over 24 h (n=4-5). (f) Rectal temperatures of mice exposed to 6° C for 2 h (n=6). For g-o, mice were fed HFD for 10-12 weeks. (g) Body weights of mice during the HFD feeding period (n=16-20). Mice were fed HFD from 6-week-old. (h-i) Glucose tolerance test results at 10 weeks of HFD feeding, including blood glucose levels and the area under the curve (AUC) (n=5-7). (j-k) Insulin tolerance test results at 11 weeks of HFD feeding (n=5-7). (l) Relative mRNA levels of thermogenesis genes in BAT (n=7). (m) UCP1 protein levels in BAT. (n-o) VO_2 of mice over 24 h (n=4). Values are means ± s.e.m. **P* < 0.05, ***P* < 0.01, and ****P* < 0.001 cf. control mice by two-tailed Student's *t*-tests.

Figure 2

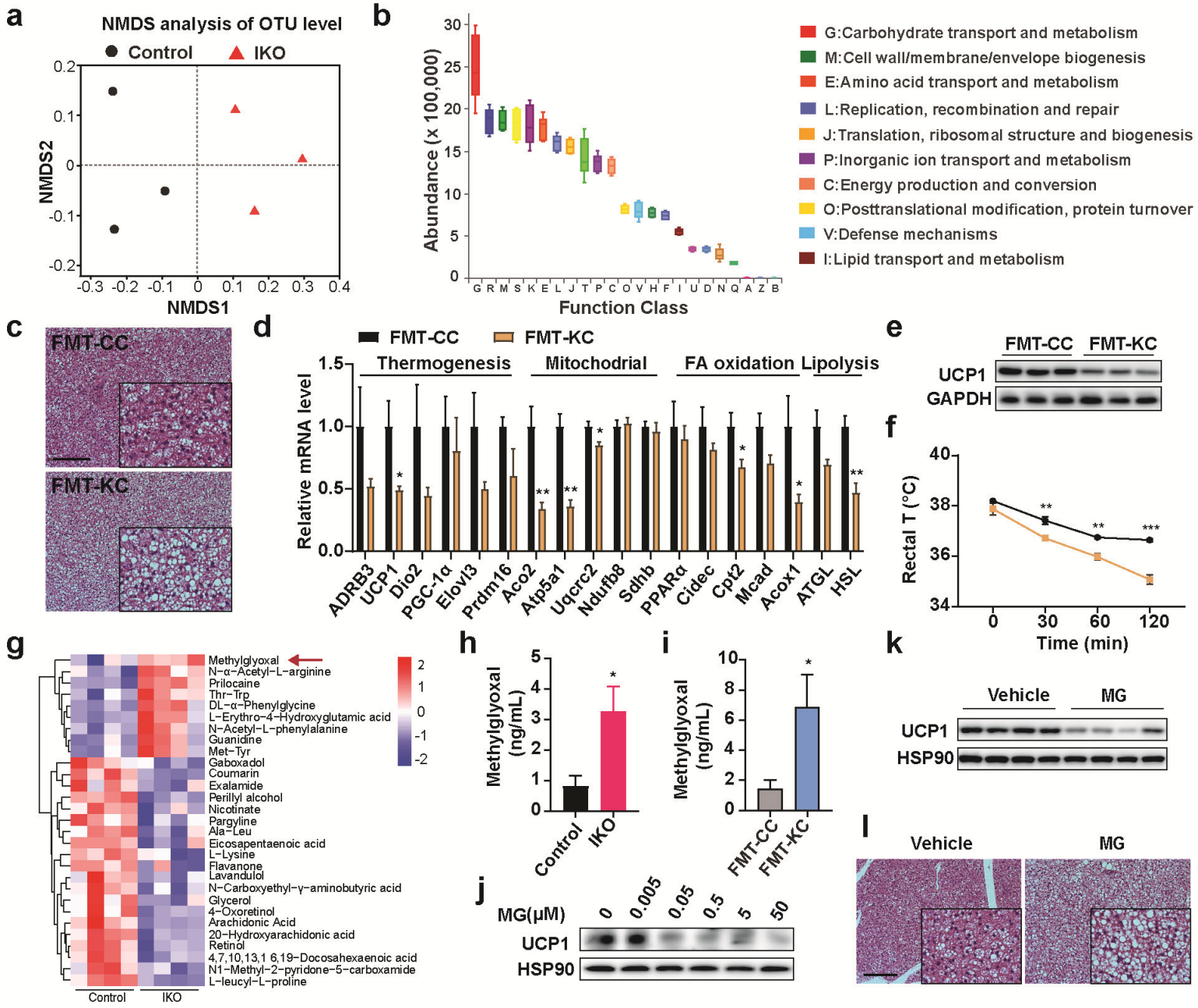

Figure 2. **Intestinal AMPK remotely controls BAT function by modulating gut microbiota and their metabolites**. (a) Non-metric multidimensional scaling (NMDS) analysis of operational taxonomic unit (OTU) levels in AMPK$^{fl/fl}$ (Control) and AMPK-IKO mice fed ND chow (n=3). (b) Functional classification of microbiota with differential abundance in AMPK-IKO mice compared to AMPK$^{fl/fl}$ mice, based on the Clusters of Orthologous Groups (COGs) database. (c) Representative images of H&E-stained BAT sections from WT FMT recipient mice. Scale bar =100 μm. FMT-CC, FMT from AMPK$^{fl/fl}$ mice to WT mice; FMT-KC, FMT from AMPK-IKO mice to WT mice. (d) Relative mRNA levels of genes expressed in the BAT of recipient mice (n=3-4). (e) Representative Western blot analysis of UCP1 protein levels in the BAT of recipient mice. (f) Rectal temperatures of mice recipient mice exposed to 6° C for 2 h (n=4-6). (g) Metabolomic analysis of serum samples from DIO Control and AMPK-IKO mice (n=4). (h-i) Serum methylglyoxal levels in DIO mice (h) and FMT recipient mice (i), measured using ELISA (n=3-4). (j) Representative Western blot analysis of UCP1 protein expression in mature HIB1B cells treated with a gradient concentration of methylglyoxal (MG) for 24 h. Experiments were performed in quadruplicate and repeated three times. (k) UCP1 protein expression in the BAT of WT mice after i.p. injections of methylglyoxal for 2 weeks (n=4). (l) Representative images of H&E-stained BAT sections of mice treated with methylglyoxal. Scale bar =100 μm. Values are means ± s.e.m. *P < 0.05, **P < 0.01 by two-tailed Student's t-tests.

Figure 3

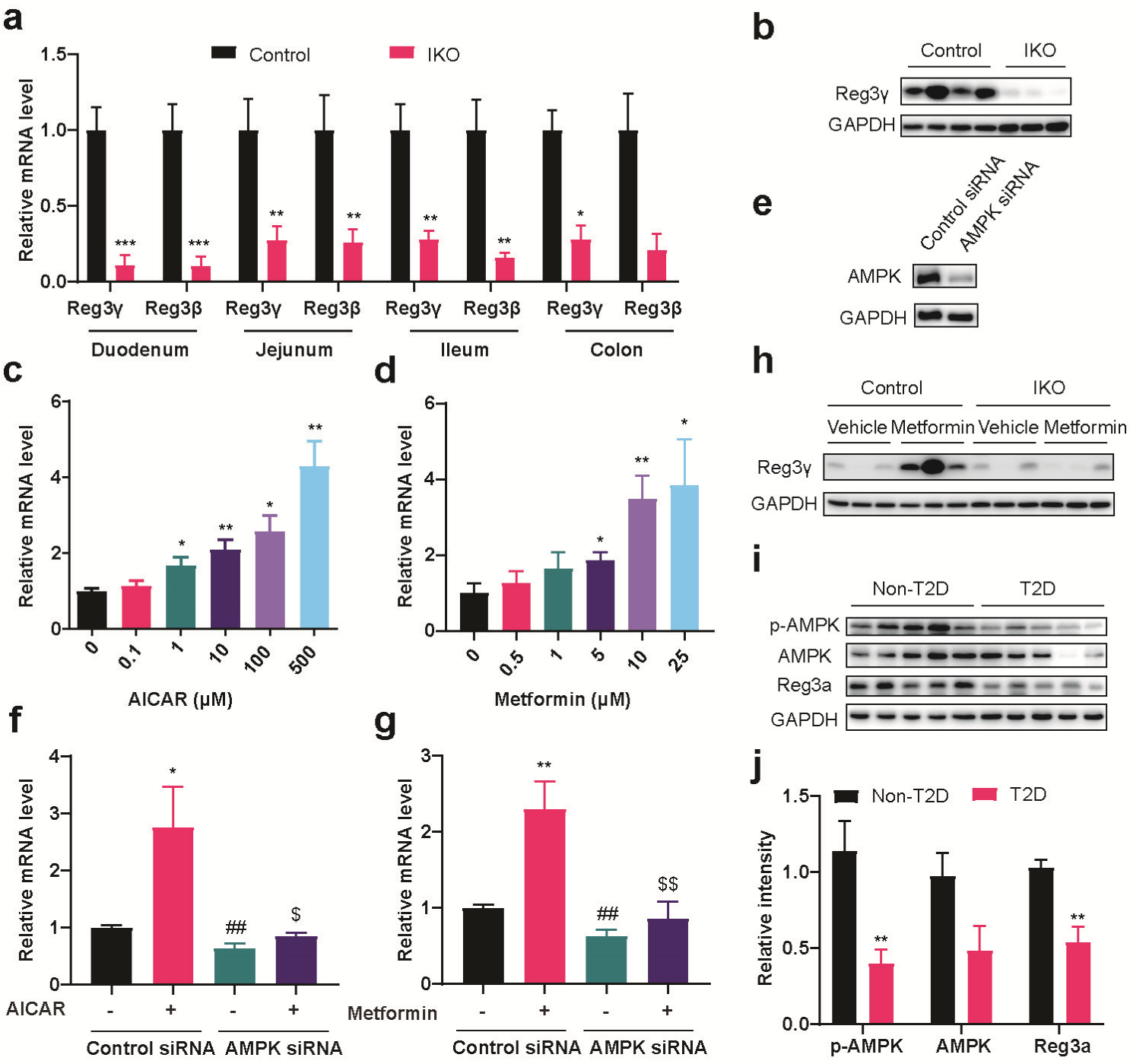

Figure 3. Intestinal AMPKα1 regulates the AMP Reg3. (a) Relative mRNA levels of Reg3γ and Reg3β in the duodenum, jejunum, ileum, and colon of AMPK$^{fl/fl}$ (Control) and AMPK-IKO mice fed ND chow (n=6). (b) Representative Reg3γ protein levels in the jejunum of mice fed ND chow. (c-d) Relative mRNA levels of Reg3α in HT-29 cells treated with gradient concentrations of AICAR (c) and metformin (d). n=4-5. (e) Western blot analysis of AMPK protein in HT-29 cells treated with control siRNA or AMPK siRNA. (f-g) Relative mRNA levels of Reg3α in AMPK knockdown HT-29 cells treated with 100 uM of AICAR (f) or 10 uM of metformin (g) for 24 h. n=6. (h) Representative Reg3γ protein levels in WT DIO mice treated with metformin. (i) Western blot analysis of total AMPK, phosphorylated AMPK (p-AMPK), and Reg3α in duodenal mucosa samples from obese patients with T2D. (j) The quantitated densities of these Western blot bands are also shown. Values are means ± s.e.m. *P < 0.05, **P < 0.01, and ***P < 0.001 by Student's t-test (for a, cf. Control mice; for c-d, cf. vehicle-treated cells; for j, cf. non-T2D human samples), and one- or two-way ANOVA with Tukey's post-hoc tests for f-g, *P < 0.05, **P < 0.01, ##P<0.01, $$P$<0.05, $$$P$<0.01. * and # cf. vehicle-treated cells infected with control siRNA, $ cf. AICAR- or metformin-treated cells infected with AMPK siRNA.

Figure 4

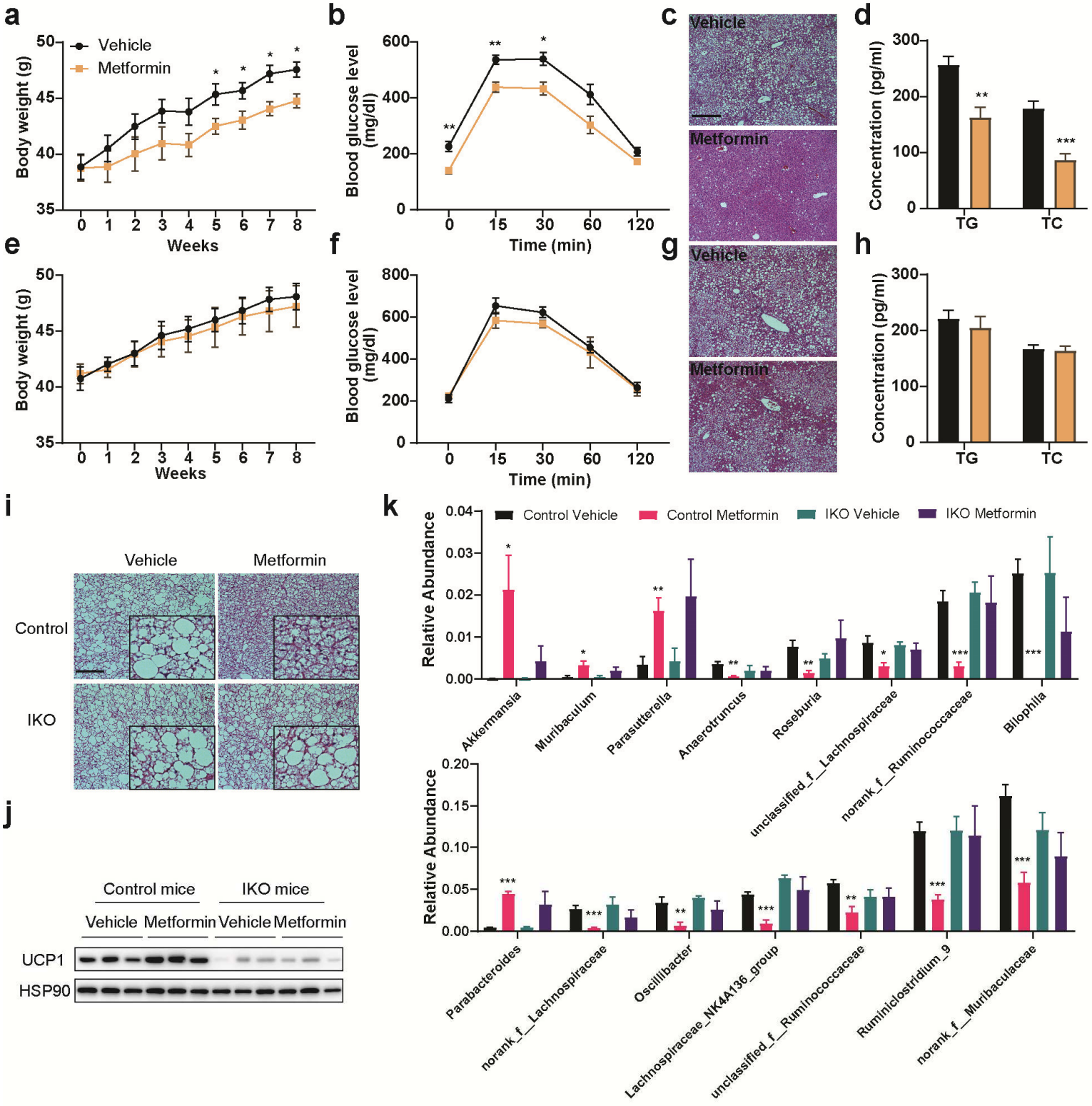

Figure 4. The therapeutic effects of metformin on metabolic disorders depend on intestinal AMPK. DIO AMPK$^{fl/fl}$ (Control; a-d) and AMPK-IKO (e-h) mice were orally garaged with metformin (100 mg/kg) once daily for 8 weeks. (a, e) Body weights of mice during metformin treatment (n=5). (b, f) Glucose tolerance test results at 8 weeks of metformin administration. (c, g) Representative images of H&E-stained liver sections. Scale bar =100 μm. (d, h) Fasting serum levels of triglycerides (TG) and total cholesterol (TC) (n=5). Values are means ± s.e.m. *P < 0.05, **P < 0.01 by two-tailed Student's t-tests. (i) Representative images of H&E-stained BAT sections. (j) Representative UCP1 protein expression in BAT. (k) Relative abundance of microbiota at the genus level (n=5). Values are means ± s.e.m. *P < 0.05, **P < 0.01, and ***P < 0.001 cf. vehicle-treated mice by one-way ANOVA with Tukey's post-hoc tests.

Figures

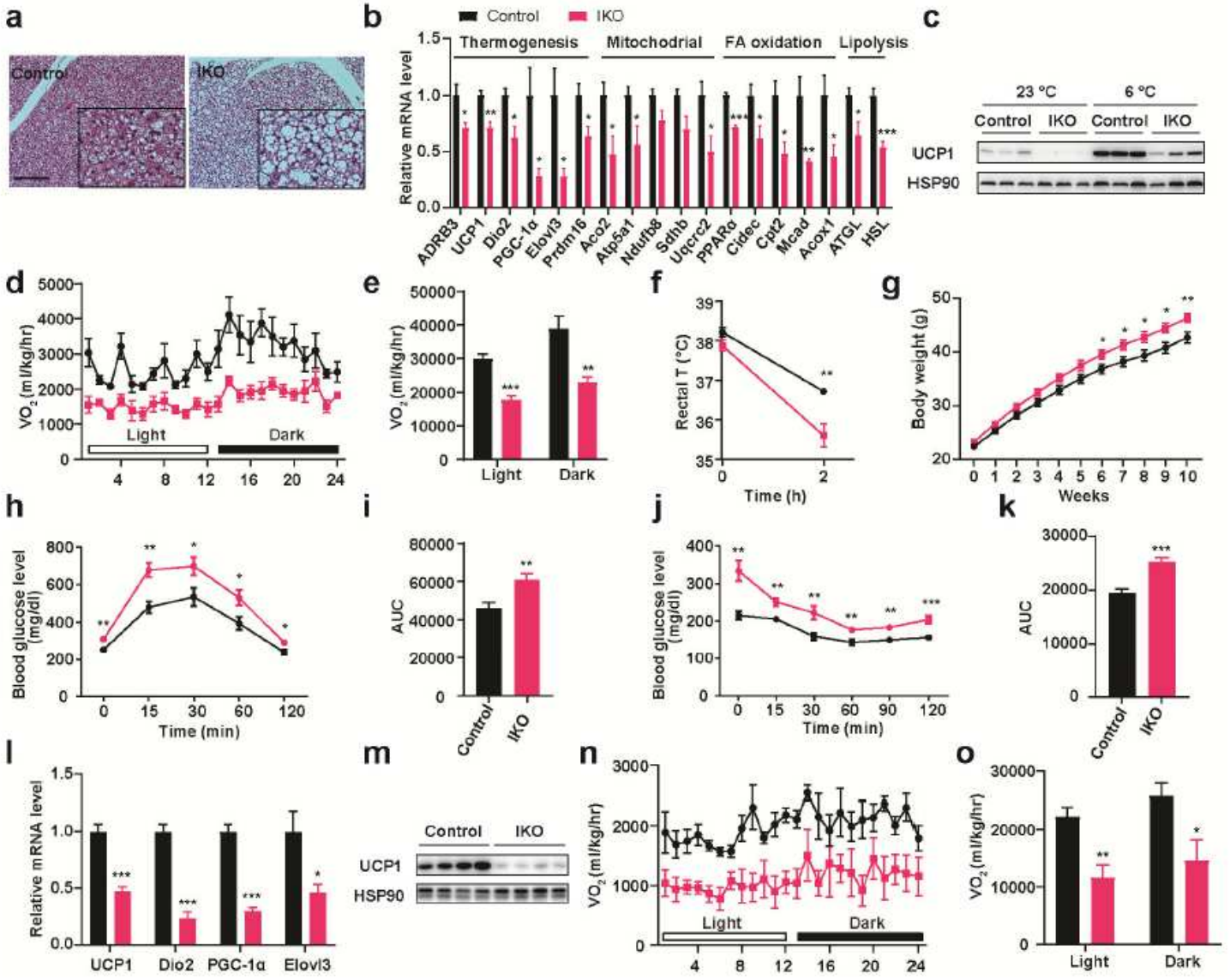

Figure 1

Intestinal epithelial AMPK knockout mice have impaired BAT function. For a-f, AMPKfl/fl (Control) and AMPK-IKO mice were fed NC. (a) Representative images of H&E-stained BAT sections. Scale bar =100 μm. (b) Relative mRNA levels of genes in BAT, detected by qPCR (n=5). (c) Western blot analysis of UCP1 protein levels in BAT before and after cold exposure (6°C) for 1 week. (d-e) VO2 of mice over 24 h (n=4-5). (f) Rectal temperatures of mice exposed to 6°C for 2 h (n=6). For g-o, mice were fed HFD for 10-12 weeks. (g) Body weights of mice during the HFD feeding period (n=16-20). Mice were fed HFD from 6-week-old. (h-i) Glucose tolerance test results at 10 weeks of HFD feeding, including blood glucose levels and the area under the curve (AUC) (n=5-7). (j-k) Insulin tolerance test results at 11 weeks of HFD feeding (n=5-7). (l) Relative mRNA levels of thermogenesis genes in BAT (n=7). (m) UCP1 protein levels in BAT. (n-o) VO2 of mice over 24 h (n=4). Values are means ± s.e.m. *P < 0.05, **P < 0.01, and ***P < 0.001 cf. control mice by two-tailed Student's t-tests.

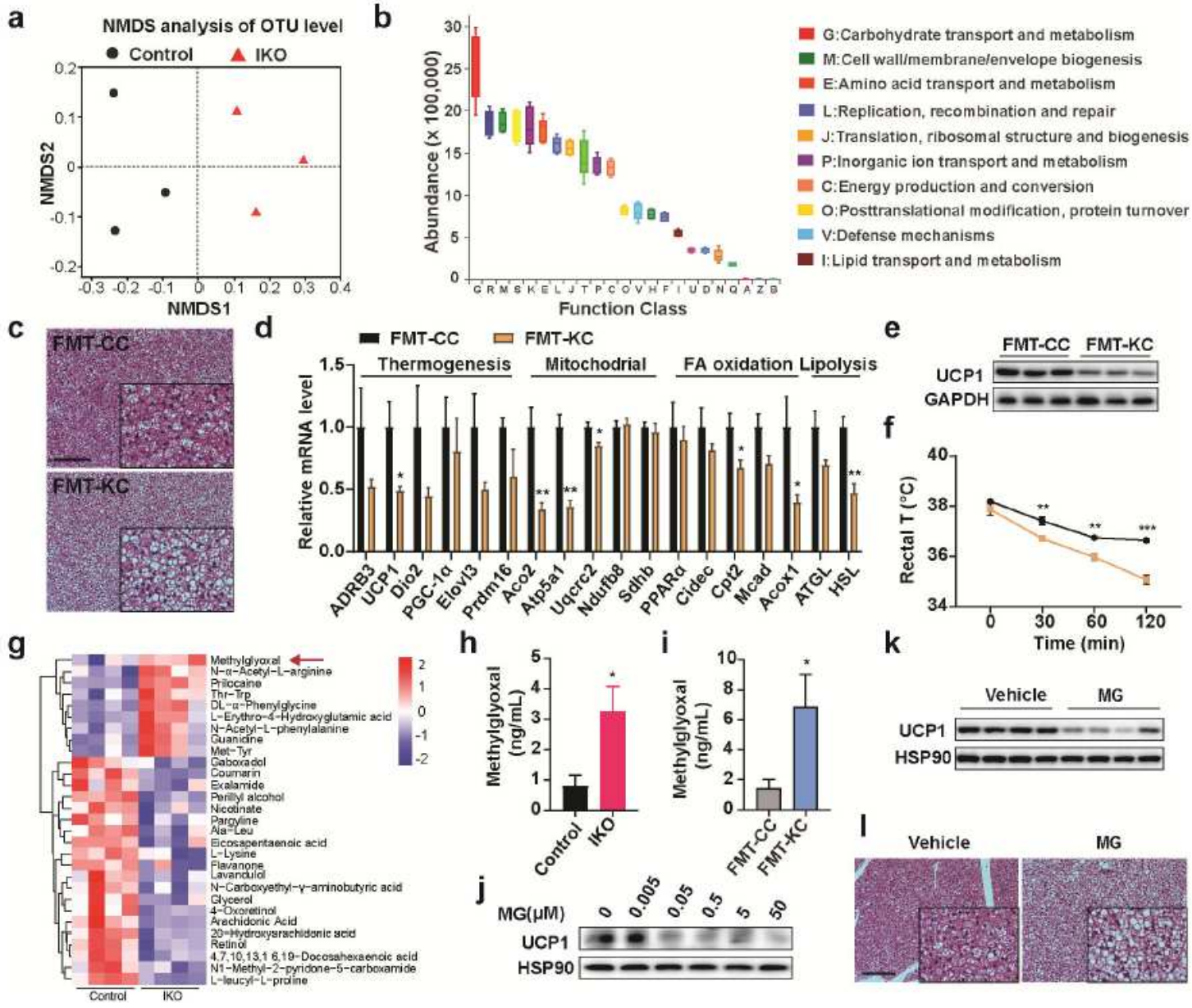

Figure 2

Intestinal AMPK remotely controls BAT function by modulating gut microbiota and their metabolites. (a) Non-metric multidimensional scaling (NMDS) analysis of operational taxonomic unit (OTU) levels in AMPKfl/fl (Control) and AMPK-IKO mice fed ND chow (n=3). (b) Functional classification of microbiota with differential abundance in AMPK-IKO mice compared to AMPKfl/fl mice, based on the Clusters of Orthologous Groups (COGs) database. (c) Representative images of H&E-stained BAT sections from WT FMT recipient mice. Scale bar =100 μm. FMT-CC, FMT from AMPKfl/fl mice to WT mice; FMT-KC, FMT from AMPK-IKO mice to WT mice. (d) Relative mRNA levels of genes expressed in the BAT of recipient mice (n=3-4). (e) Representative Western blot analysis of UCP1 protein levels in the BAT of recipient mice. (f) Rectal temperatures of mice recipient mice exposed to 6°C for 2 h (n=4-6). (g) Metabolomic analysis of serum samples from DIO Control and AMPKIKO mice (n=4). (h-i) Serum methylglyoxal levels in DIO mice (h) and FMT recipient mice (i), measured using ELISA (n=3-4). (j) Representative Western blot

analysis of UCP1 protein expression in mature HIB1B cells treated with a gradient concentration of methylglyoxal (MG) for 24 h. Experiments were performed in quadruplicate and repeated three times. (k) UCP1 protein expression in the BAT of WT mice after i.p. injections of methylglyoxal for 2 weeks (n=4). (l) Representative images of H&E-stained BAT sections of mice treated with methylglyoxal. Scale bar =100 μm. Values are means ± s.e.m. *P < 0.05, **P < 0.01 by two-tailed Student's t-tests.

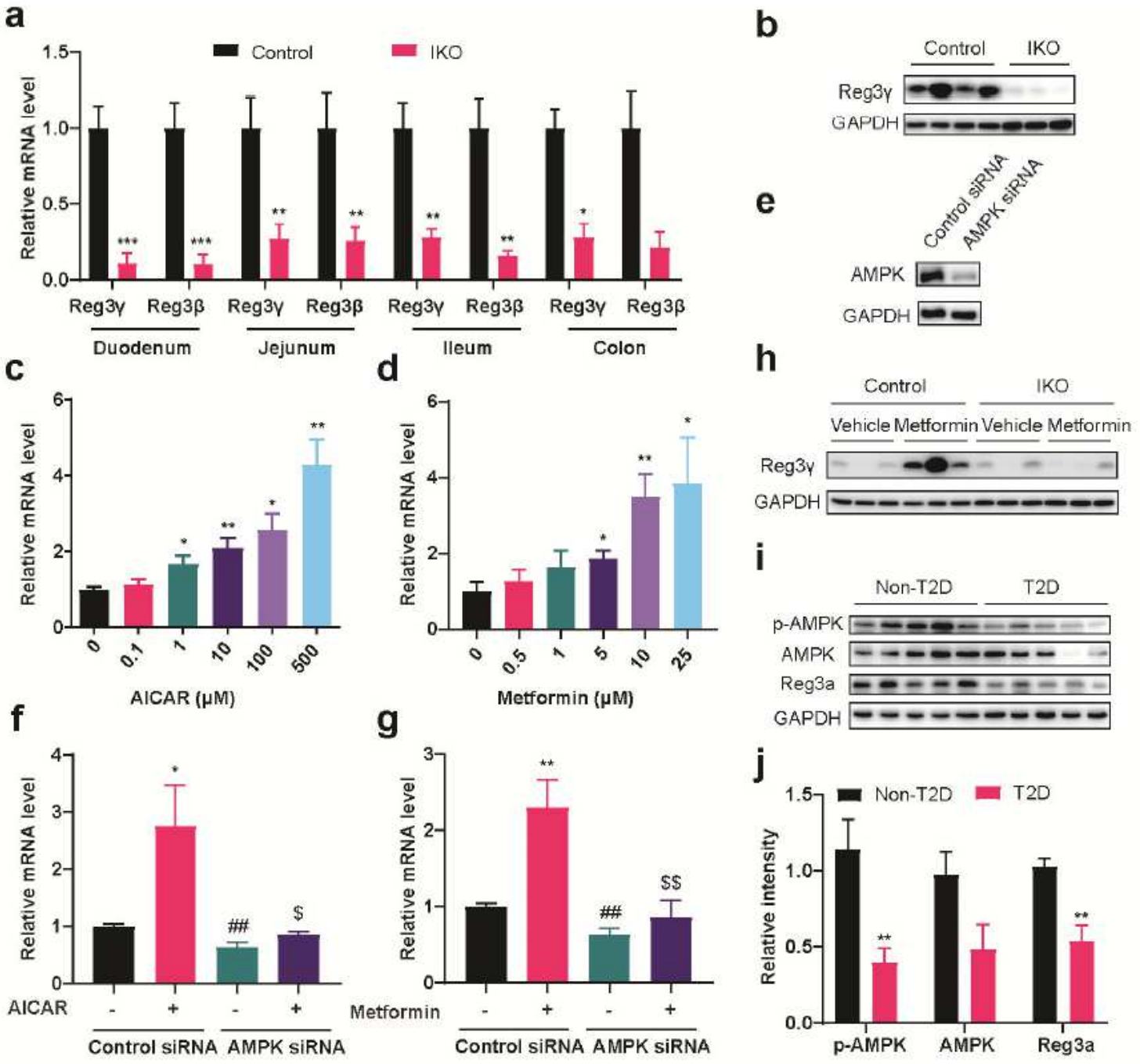

Figure 3

Intestinal AMPKα1 regulates the AMP Reg3. (a) Relative mRNA levels of Reg3γ and Reg3β in the duodenum, jejunum, ileum, and colon of AMPKfl/fl (Control) and AMPK-IKO mice fed ND chow (n=6). (b) Representative Reg3γ protein levels in the jejunum of mice fed ND chow. (c-d) Relative mRNA levels of

Reg3α in HT-29 cells treated with gradient concentrations of AICAR (c) and metformin (d). n=4-5. (e) Western blot analysis of AMPK protein in HT-29 cells treated with control siRNA or AMPK siRNA. (f-g) Relative mRNA levels of Reg3α in AMPK knockdown HT-29 cells treated with 100 uM of AICAR (f) or 10 uM of metformin (g) for 24 h. n=6. (h) Representative Reg3γ protein levels in WT DIO mice treated with metformin. (i) Western blot analysis of total AMPK, phosphorylated AMPK (p-AMPK), and Reg3α in duodenal mucosa samples from obese patients with T2D. (j) The quantitated densities of these Western blot bands are also shown. Values are means ± s.e.m. *P < 0.05, **P < 0.01, and ***P < 0.001 by Student's t-test (for a, cf. Control mice; for c-d, cf. vehicle-treated cells; for j, cf. non-T2D human samples), and one- or two-way ANOVA with Tukey's post-hoc tests for f-g, *P < 0.05, **P < 0.01, ##P<0.01, $P<0.05, $$P<0.01. * and # cf. vehicle-treated cells infected with control siRNA, $ cf. AICAR- or metformin-treated cells infected with AMPK siRNA.

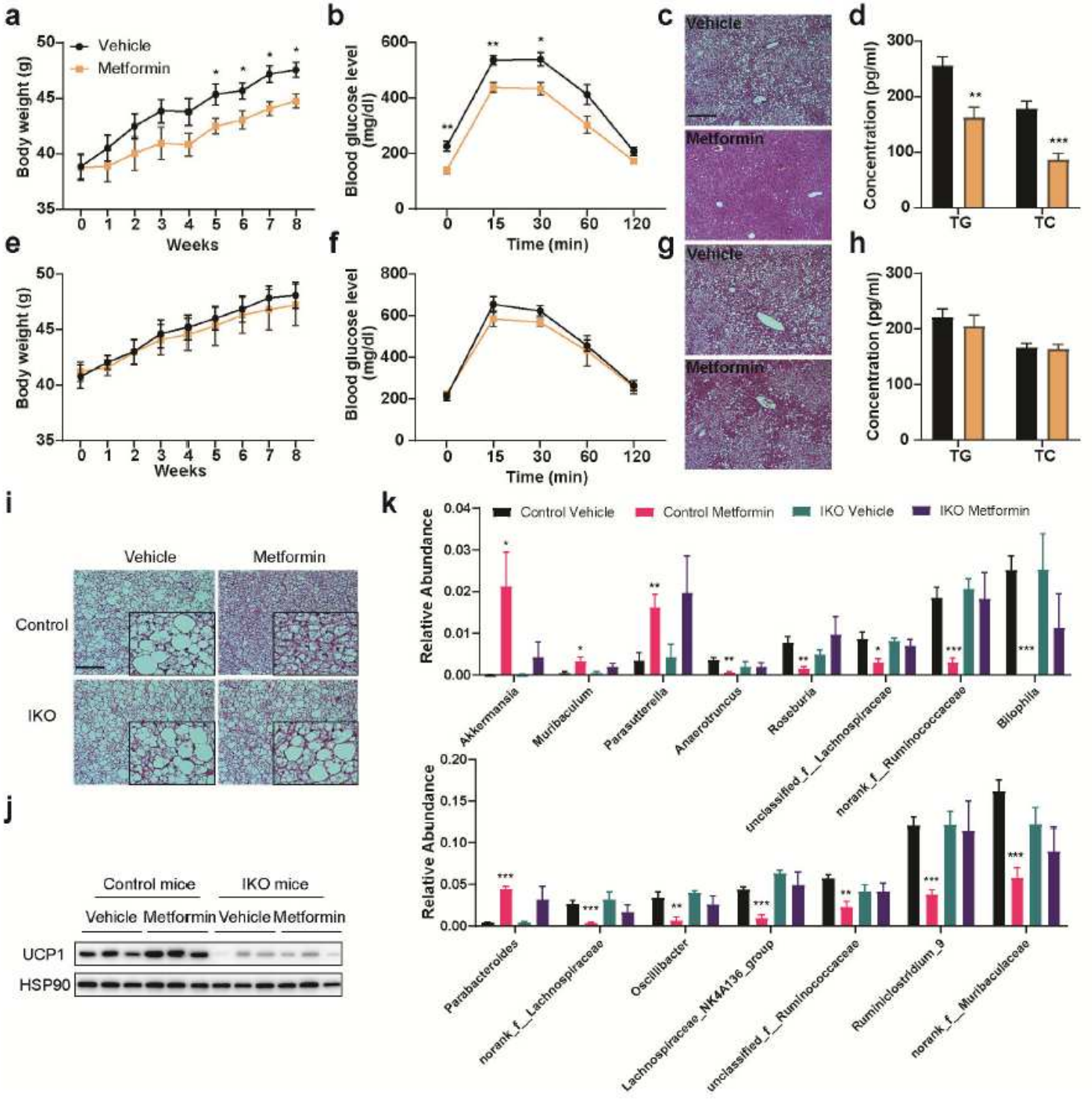

Figure 4

The therapeutic effects of metformin on metabolic disorders depend on intestinal AMPK. DIO AMPKfl/fl (Control; a-d) and AMPK-IKO (e-h) mice were orally garaged with metformin (100 mg/kg) once daily for 8 weeks. (a, e) Body weights of mice during metformin treatment (n=5). (b, f) Glucose tolerance test results at 8 weeks of metformin administration. (c, g) Representative images of H&E-stained liver sections. Scale bar =100 μm. (d, h) Fasting serum levels of triglycerides (TG) and total cholesterol (TC) (n=5). Values are means ± s.e.m. *P < 0.05, **P < 0.01 by two-tailed Student's t-tests. (i) Representative images of H&E-

stained BAT sections. (j) Representative UCP1 protein expression in BAT. (k) Relative abundance of microbiota at the genus level (n=5). Values are means ± s.e.m. *P < 0.05, **P < 0.01, and ***P < 0.001 cf. vehicle-treated mice by one-way ANOVA with Tukey's post-hoc tests.

Supplementary Files

This is a list of supplementary files associated with this preprint. Click to download.

- ZhangSupplementaryInformation11232020.pdf